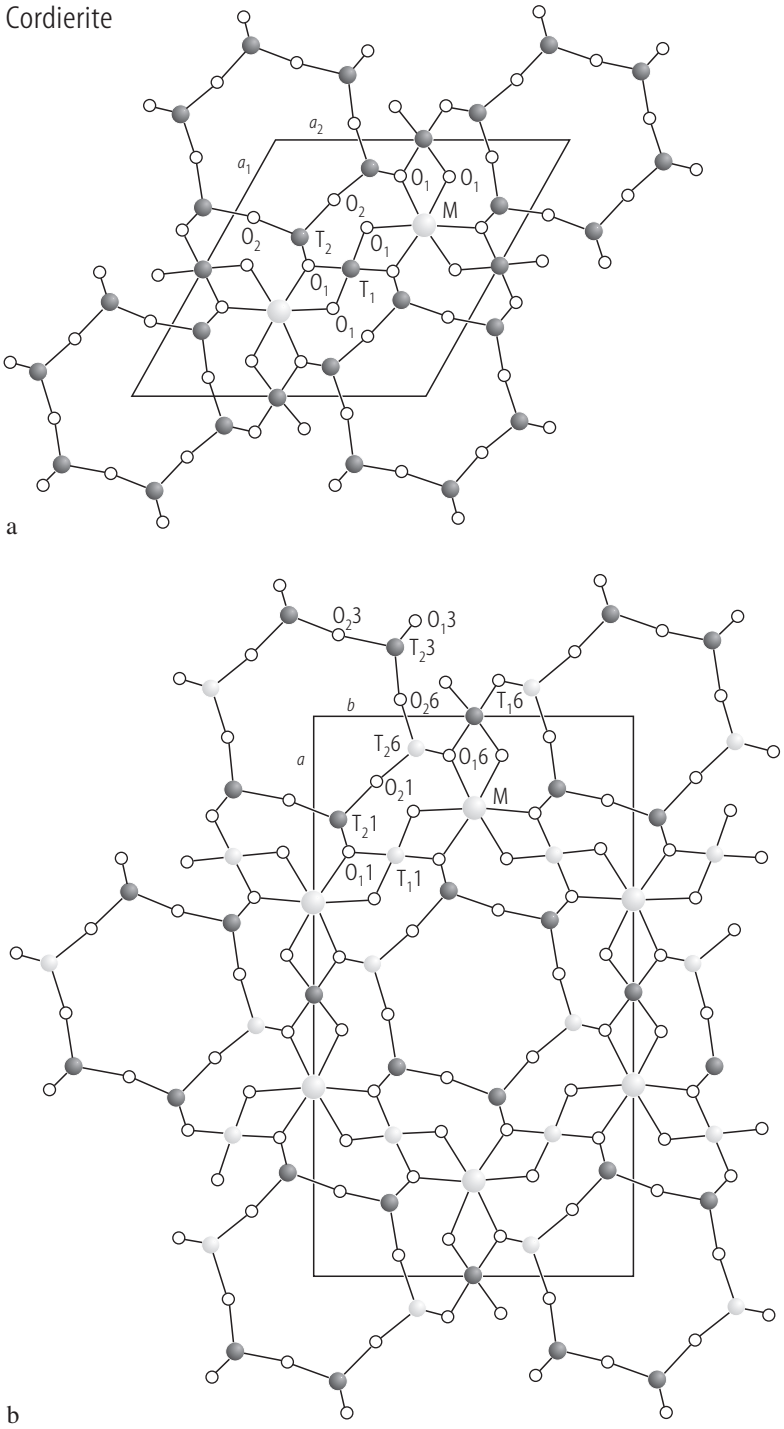

Fig. 1. Cordierites. ***c***-axis projection of **(a)** hexagonal form and **(b)** idealized orthorhombic form. In hexagonal structure T_1 sites are Si-rich and T_2 are Al-rich. In the orthorhombic low cordierite structure, full T_1, T_2 circles are Si and open T_1, T_2 circles are Al [77M1].

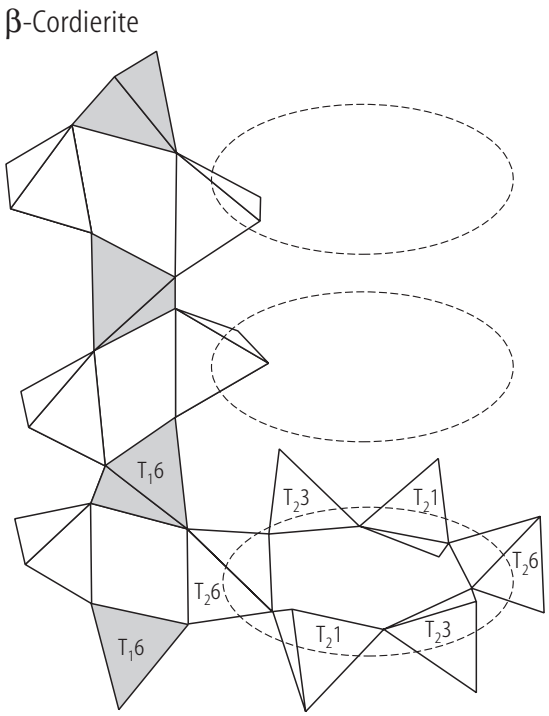

Fig. 2. β-Cordierite. The arrangement of tetrahedra. Each T_2 tetrahedron in the rings is joined via a T_1 tetrahedron (shaded) to the ring above and the ring below, such that all tetrahedra are corner sharing. The dashed lines show the position of similar rings of T_2 tetrahedra forming channels, only one of which is shown along the ***c***-axis [85P1].

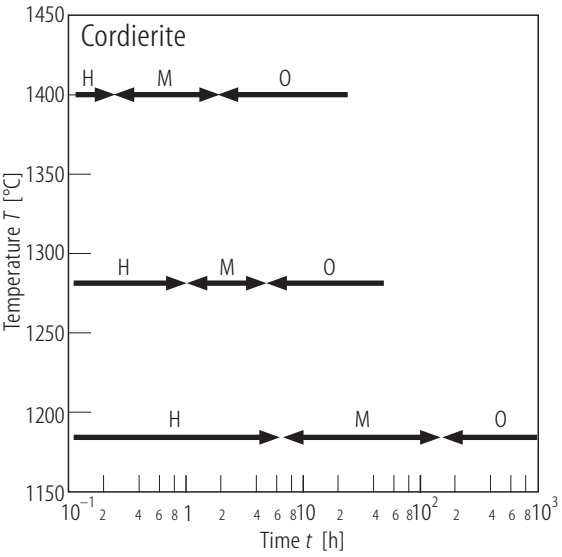

Fig. 4. Cordierites. Time-temperature diagram for the formation of three different corderite phases by dry annealing corderite glass [87P2] (H – hexagonal, M – modulated, O – orthorhombic).

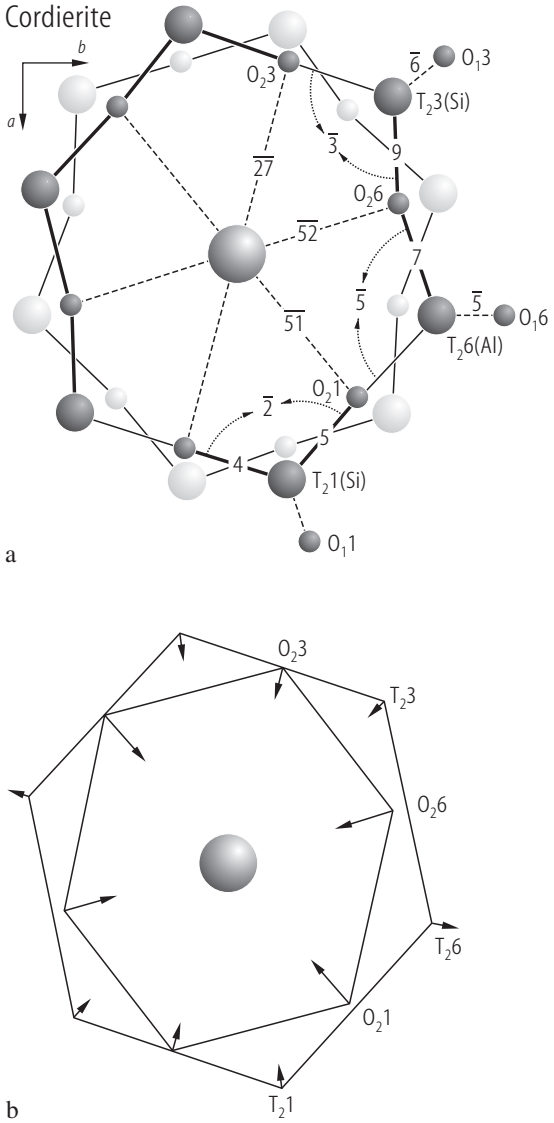

Fig. 3. Low cordierite. Distortion of the six-membered rings of tetrahedra owing to Na incorporation. **(a)** Ring at $z = 0$ is emphasized by connection of dark shaded circles centered by Na at Ch0 (site symmetry 222). Light shaded circles indicate atom positions at $z = \pm 1/2$. Decrease of Ch0–O distances owing to Na in Ch0 is indicated by dashed lines. The amount of change is given in 0.001 Å. Heavy solid lines specify increased anion-cation distances. Decrease of T–O–T angles is shown by dotted curves given for each angle. The change of angles is in full degrees. **(b)** Oxygen atoms at $z = 0$ are connected with each other to form an inner ring. Also shown are cations at $z = 0$ to form an outer ring. Arrows indicate the relative motion due to Na incorporation. The oxygen ring contracts mainly along the vector Na–$T_2$6, whereas the cation ring expands along this direction [86A2].

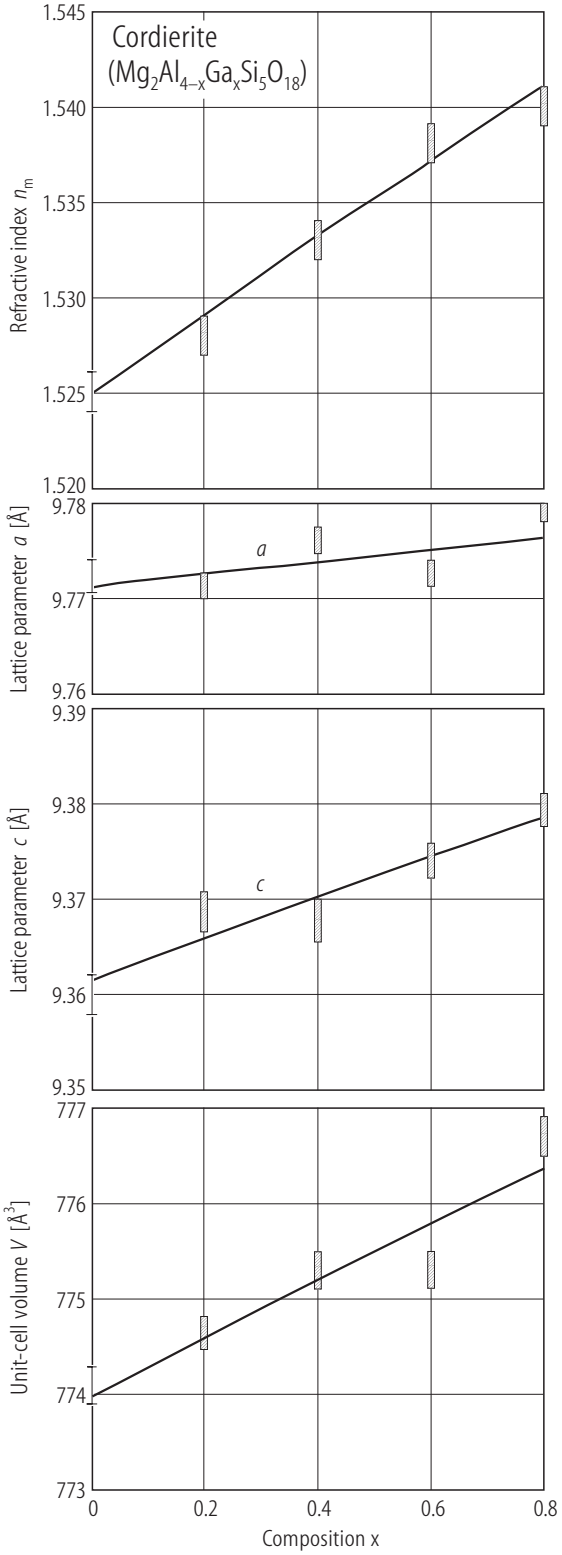

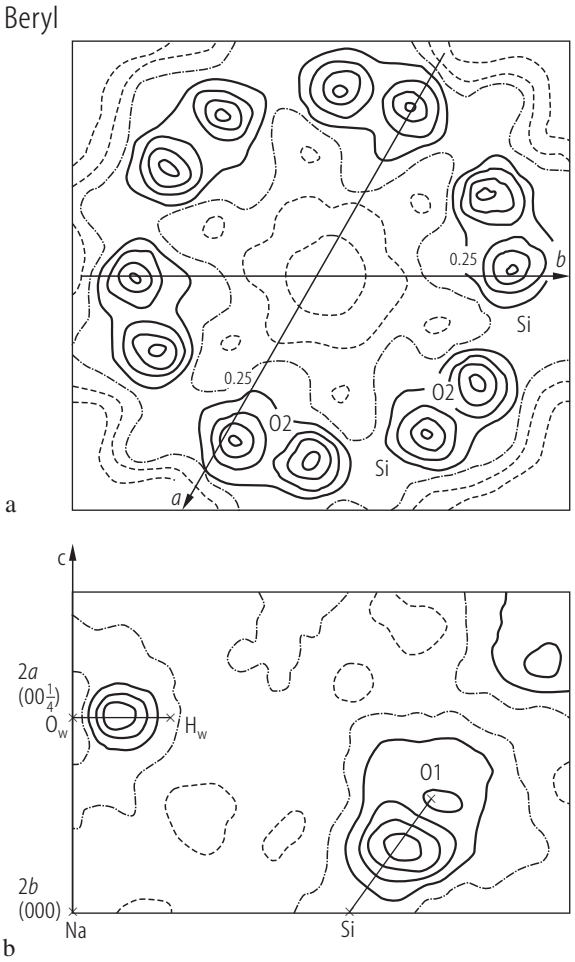

Fig. 7. Beryl[40]. **(a)** $\delta\rho$ map through $[Si_6O_{18}]^{12-}$ ring. **(b)** $\delta\rho$ map through hexagonal channel and O1–O1 edge of SiO_4 tetrahedron [88E1]. Contours spacing 0.1 eÅ^{-3}.

For Fig. 6 see next page

←

Fig. 5. Ga-bearing cordierites. Lattice parameters and unit cell volume as function of composition [71L1]. The samples were obtained through devitrification of glasses at 1 atm and 1050 ^{0}C/110 h. The refractive index is also given.

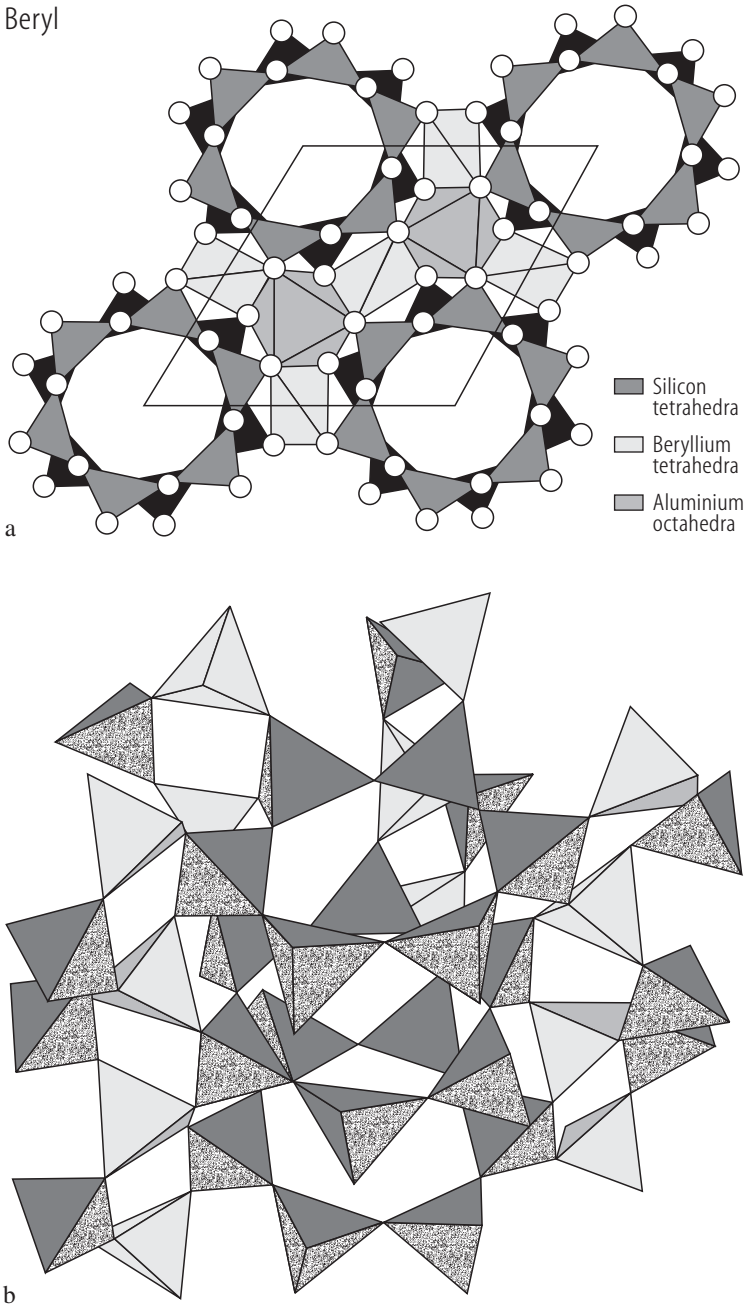

Fig. 6. Beryl. Crystal structure [68G1]. **(a)** The ***c***-axis projection shows the six-membered tetrahedral rings of Si, which are cross-linked by Be tetrahedra and Al octahedra. **(b)** The arrangement of Si and Be tetrahedra resulting in a continuous three-dimensional framework.

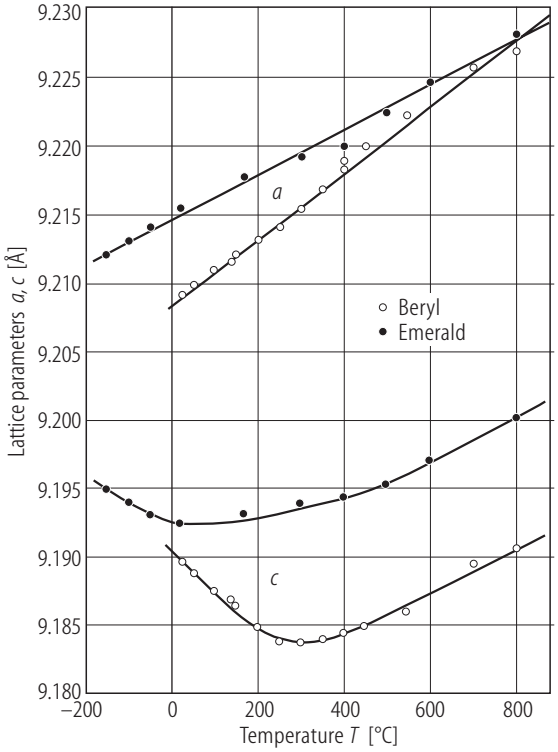

Fig. 8. Beryl[36] (o) and emerald[41] (•). Temperature dependences of the lattice parameters [72M1]. Smooth curves have been drawn through the points for the ***c***-axes and straight lines were drawn through the points for the ***a***-axes.

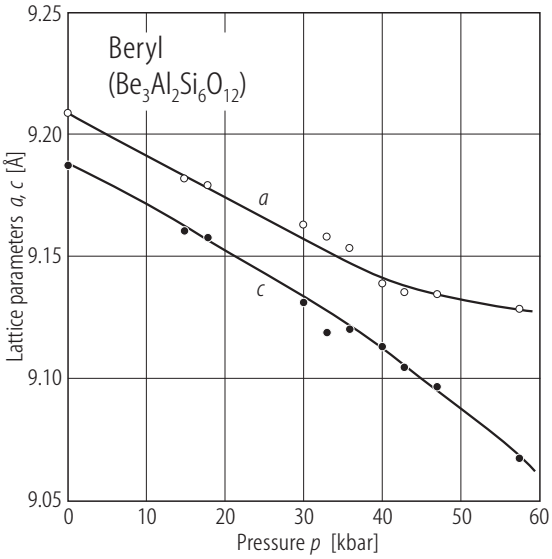

Fig. 9. Beryl[42]. Pressure dependences of lattice parameters [86H1].

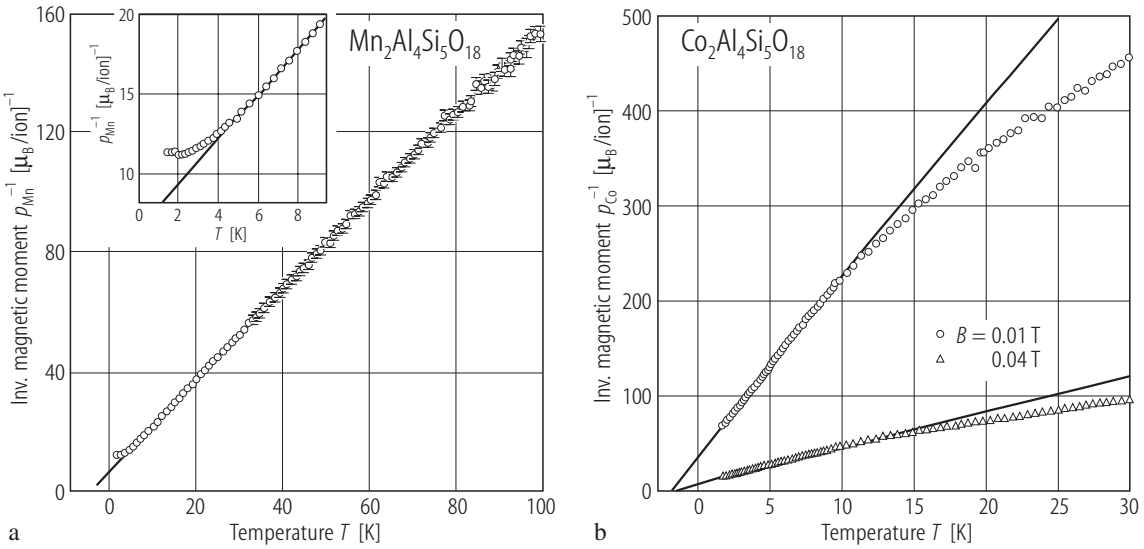

Fig. 10. $Mn_2Al_4Si_5O_{18}$ **(a)**, $Co_2Al_4Si_5O_{18}$ **(b)** cordierites. Temperature dependences of the inverse magnetic moments [99K1]. The solid lines in **(b)** correspond to the fit of the paramagnetic Curie-Weiss law for $T < 10$ K

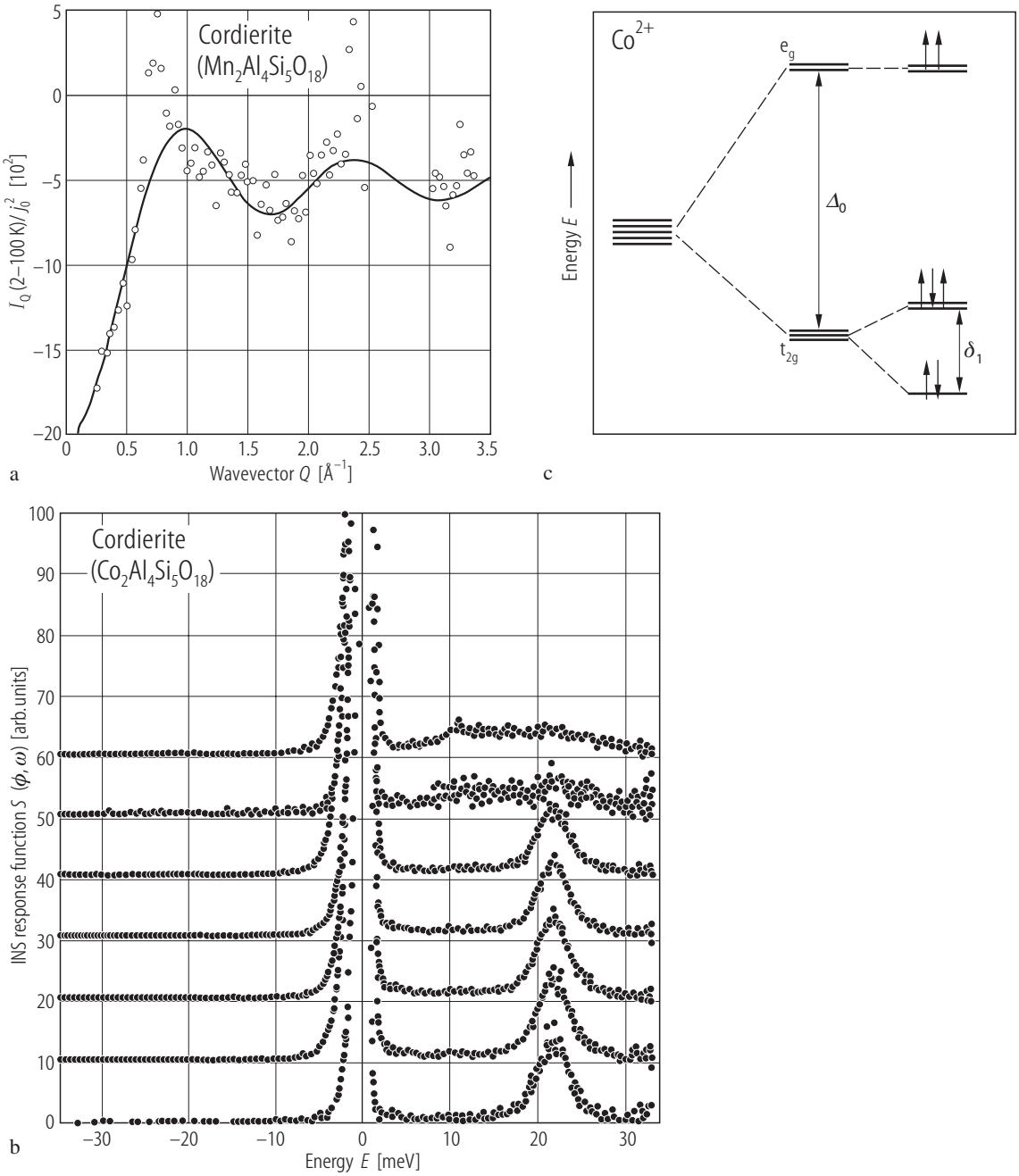

Fig. 12. $Mn_2Al_4Si_5O_{18}$ cordierite **(a)**. Fit of a Blech-Averbach function for Mn^{2+} nearest neighbour interaction through the normalized difference signal $I_Q(2–100)/j_0^2$. I_Q/j_0^2 is the magnetic scattering intensity as function of the scattering vector $Q = 2\pi\sin\theta/\lambda$ normalized by the magnetic form factor j_0 [99K1]. – $Co_2Al_4Si_5O_{18}$ cordierite **(b)**. Magnetic scattering [97W1]. **(c)** The splitting of the 3d-orbitals. The relative energy levels due to octahedral coordination (center) and the splitting for a trigonal distortion (right hand side) are given [93B1, 97W1].

For Fig. 11 see next page

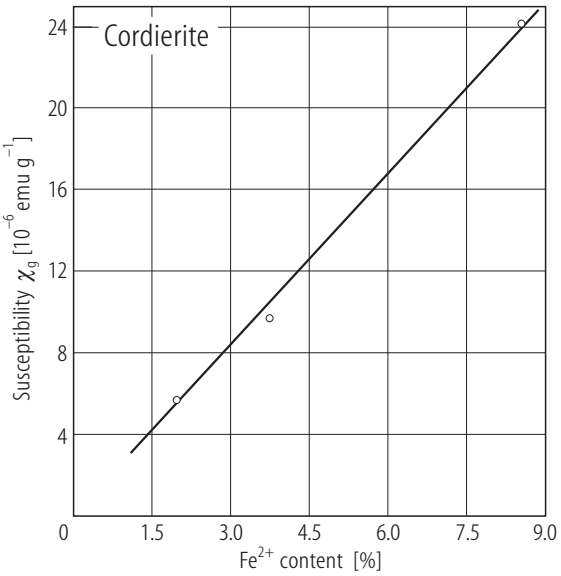

Fig. 11. Cordierites. Magnetic susceptibilities versus Fe^{2+} content [68P1].

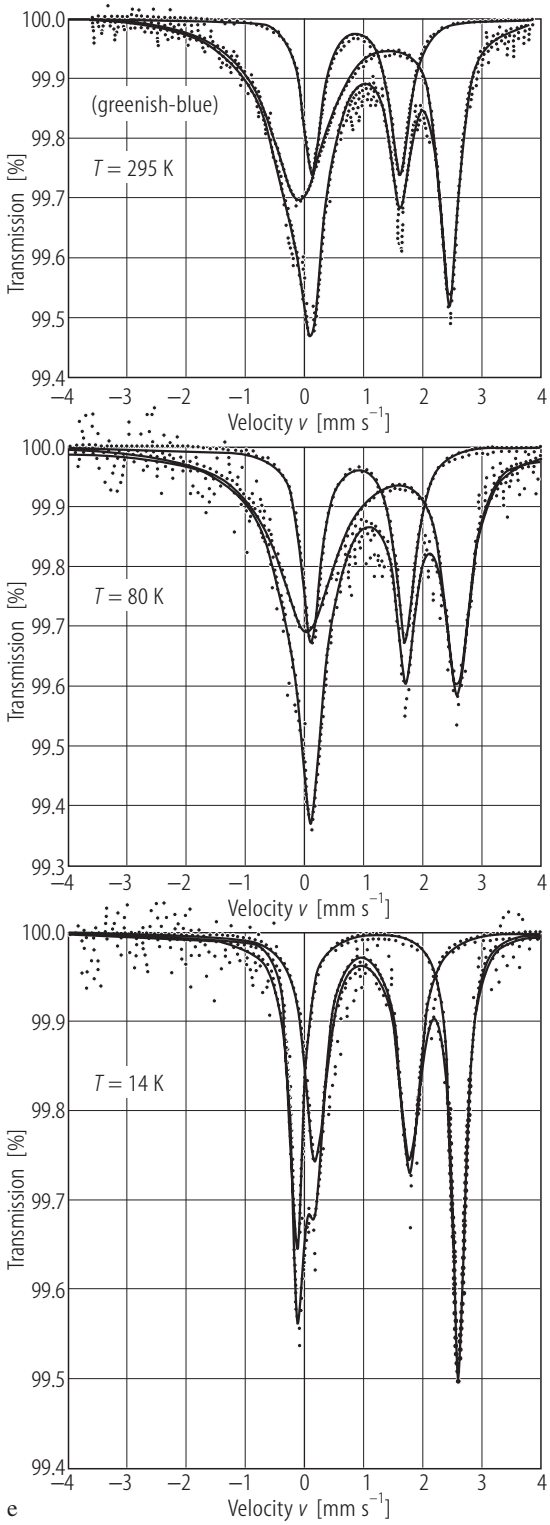

e

Fig. 13e.

Fig. 13. Beryls. ^{57}Fe NGR spectra. Deep blue beryl at **(a)** 4.2, 30 and 295 K (type I fit) and **(b)** type II fit at 4.2 and 295 K; **(c)** light blue beryl at 14 and 295 K; **(d)** bluish green beryl at 80 and 295 K; **(e)** greenish blue beryl at 14, 80 and 295 K [02V1].

For Figs. 13a, b, c, d see next pages

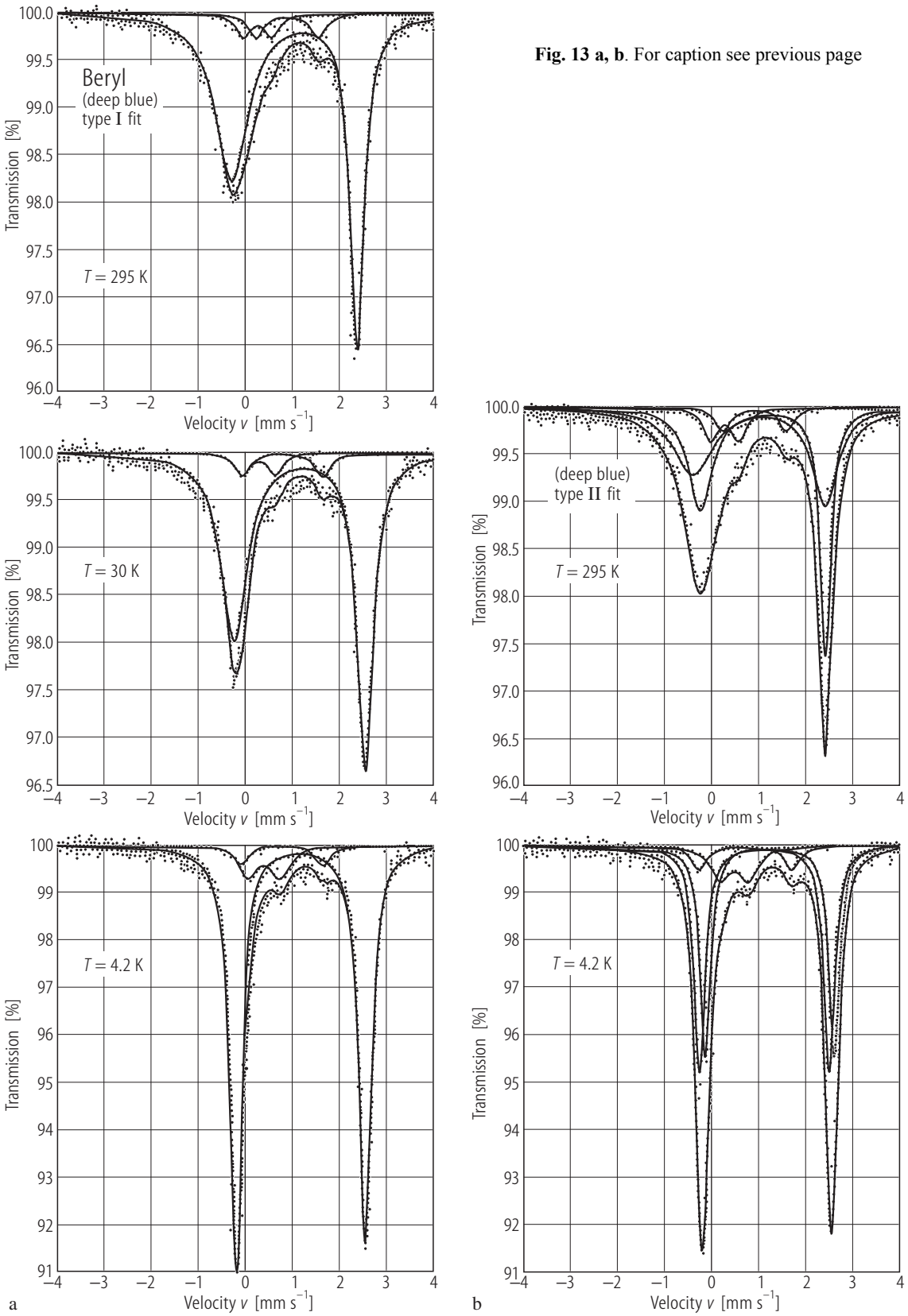

Fig. 13 a, b. For caption see previous page

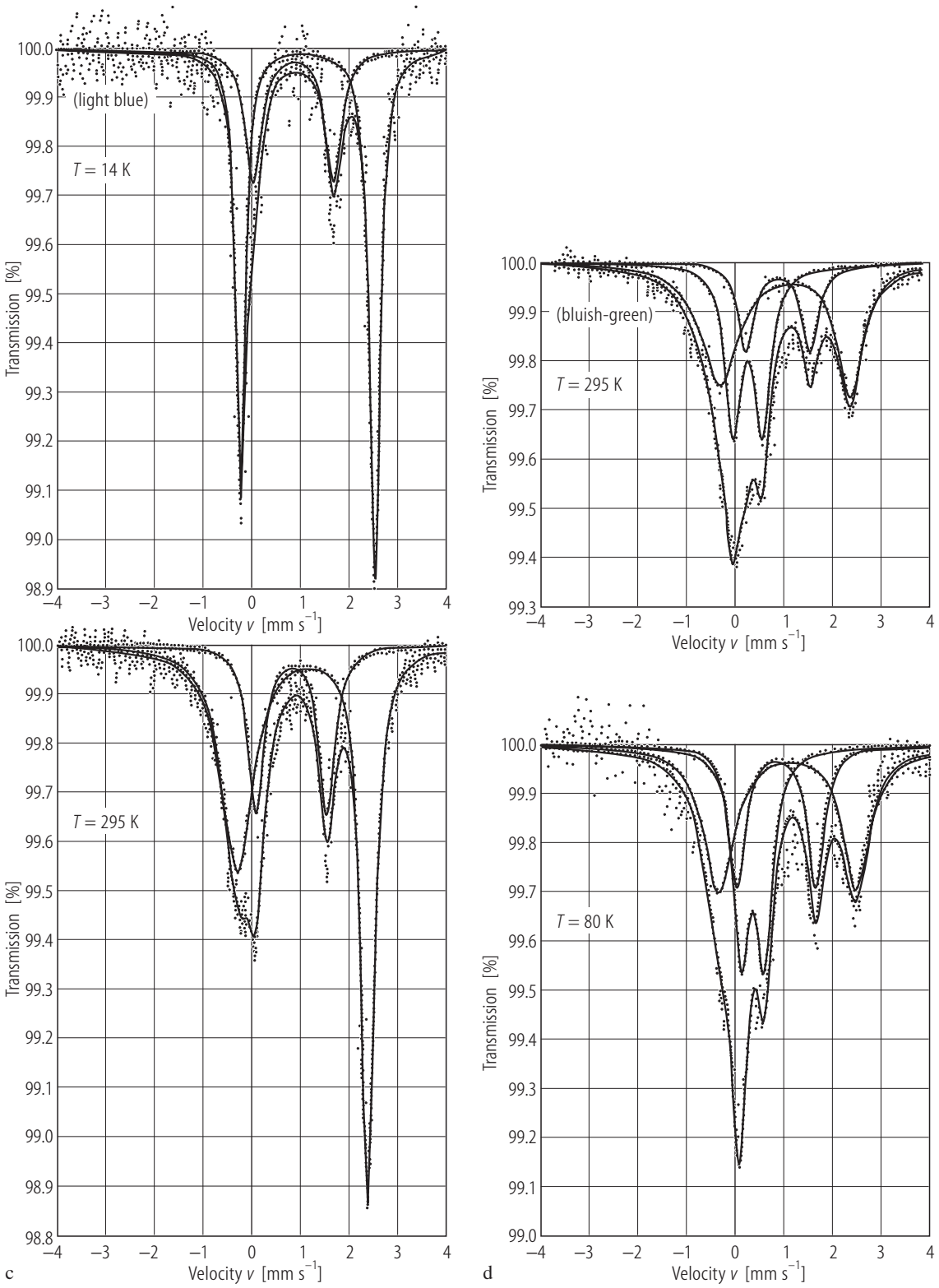

Fig. 13c, d. For caption see p. 104.

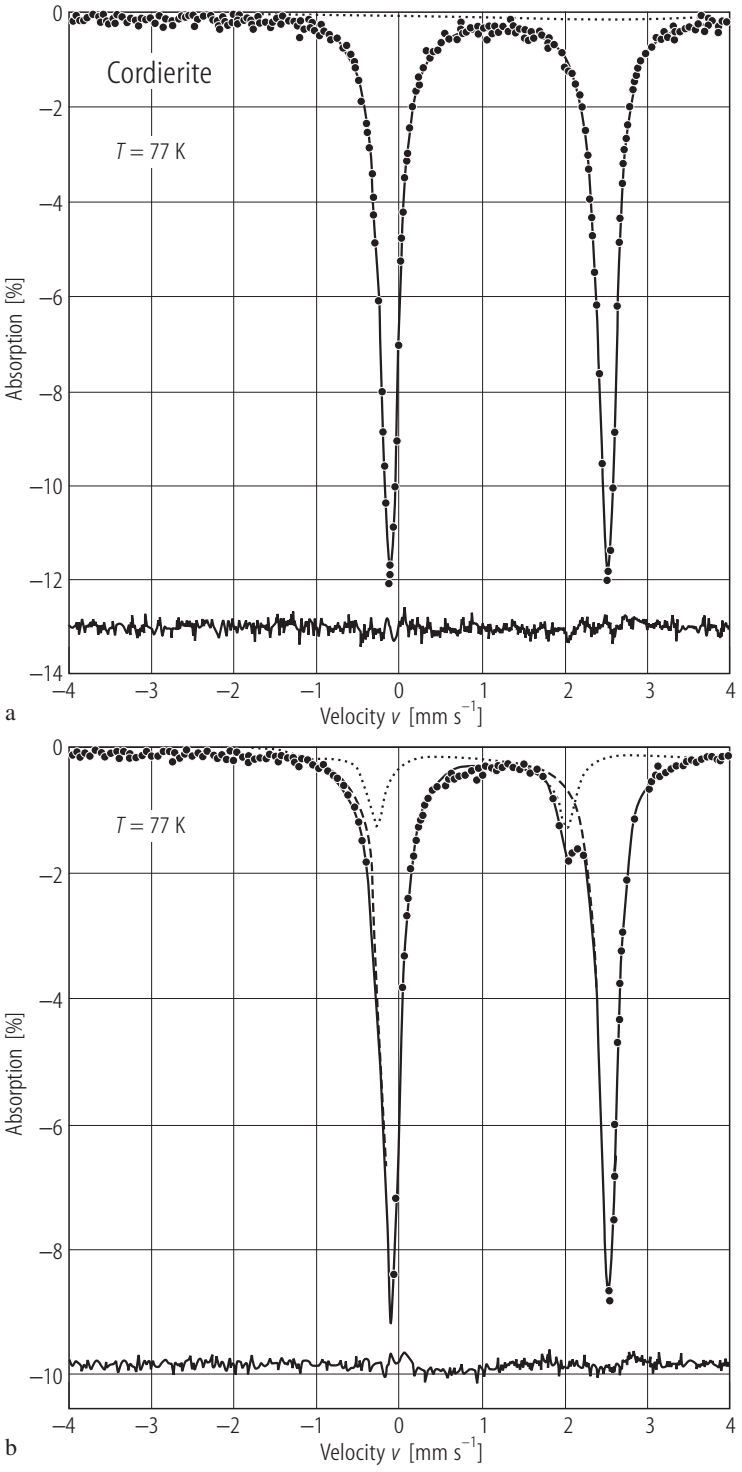

Fig. 14. Cordierite. ^{57}Fe NGR spectra at 77 K: **(a)** natural sample[33)], **(b)** natural sample[32)] (compositions according to Table 3) [00G1].

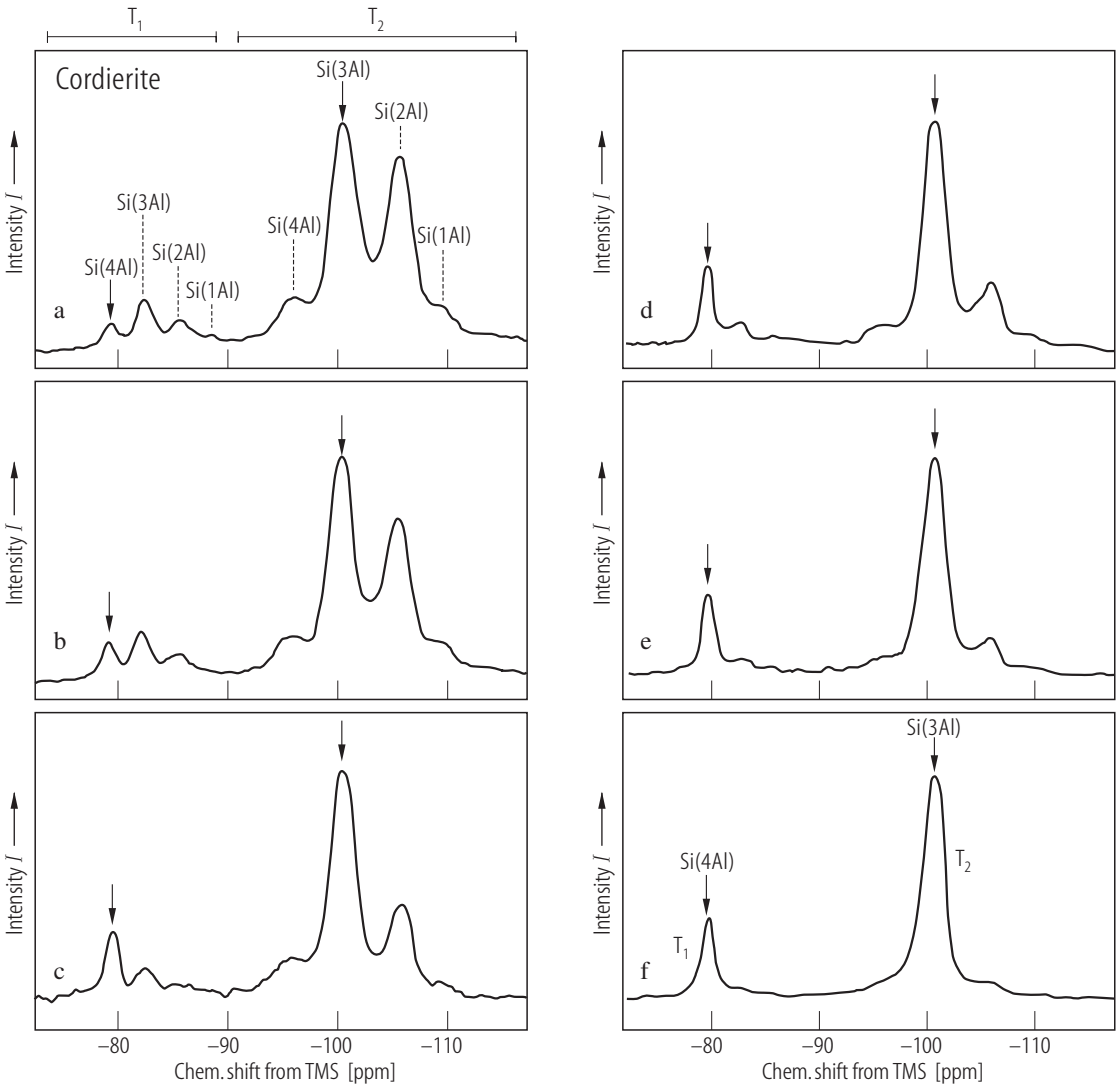

Fig. 15. Cordierite, $Mg_2Al_4Si_5O_{18}$. A sequence **(a-f)** of ^{29}Si NMR spectra of synthetic samples annealed for increasing time [87P2]. In **(a)** the large number of Si(nAl) environments is due to the disorder in the first formed hexagonal phase, while in **(f)** the orthorhombic cordierite is well ordered.

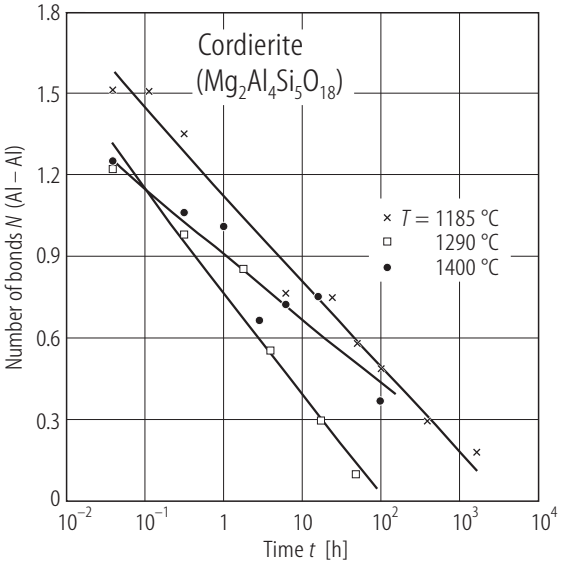

Fig. 16. Cordierite, $Mg_2Al_4Si_5O_{18}$. The number of Al–O–Al bonds per formula unit plotted as function of annealing time at three different temperatures [87P2].

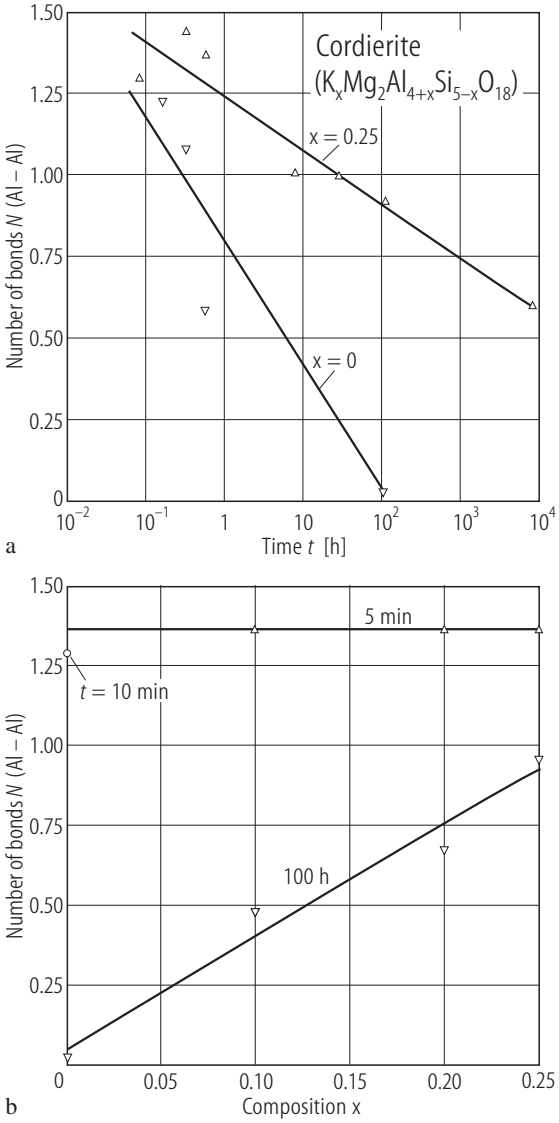

Fig. 17. $K_xMg_2Al_{4+x}Si_{5-x}O_{18}$ cordierites. **(a)** The number of Al–O–Al bonds per formula unit for samples with x = 0 and x = 0.25 as a function of the logarithm of annealing time. The speed of ordering is much slower for cordierites with x = 0.25 than for x = 0. The estimated errors of all values shown are ±0.03. **(b)** The number of Al–O–Al bonds per formula unit after two different annealing times as a function of the K-concentration [92D1].

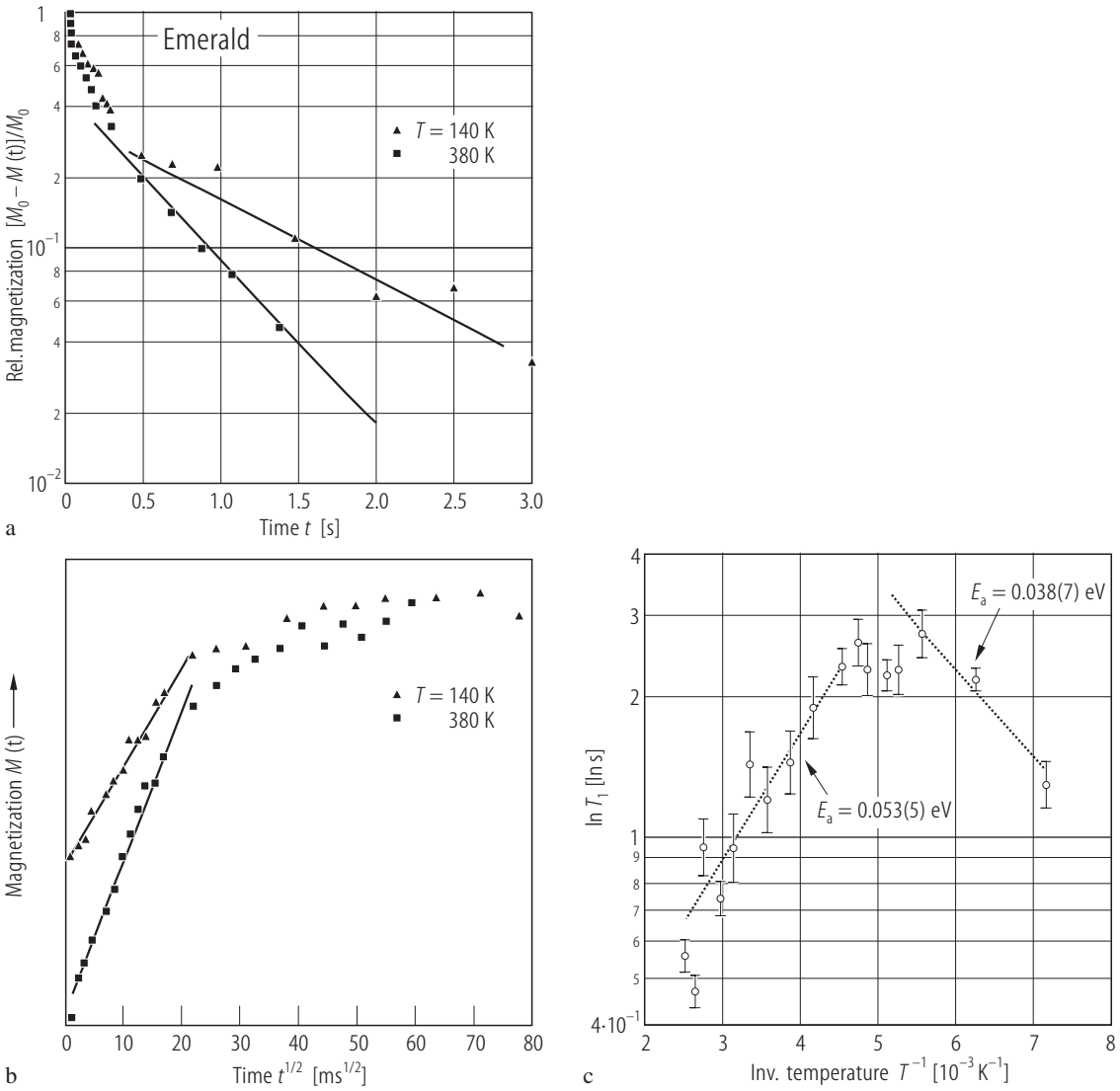

Fig. 18. Emerald[40] single crystal. Data obtained from ^{27}Al NMR. **(a)** The reduced magnetization (represented by the signal intensity in logarithmic scale) versus delay time, t. **(b)** The magnetization recovery curves at 140 and 380 K. M_0 is the saturated magnetization when the delay time is long enough [00K1]. **(c)** Temperature dependence of the spin-lattice relaxation time of the ^{27}Al nucleus. The activation energies are also given [00K1].

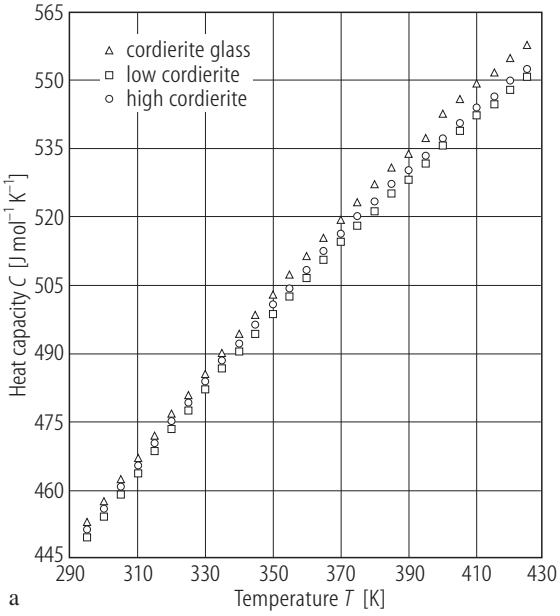

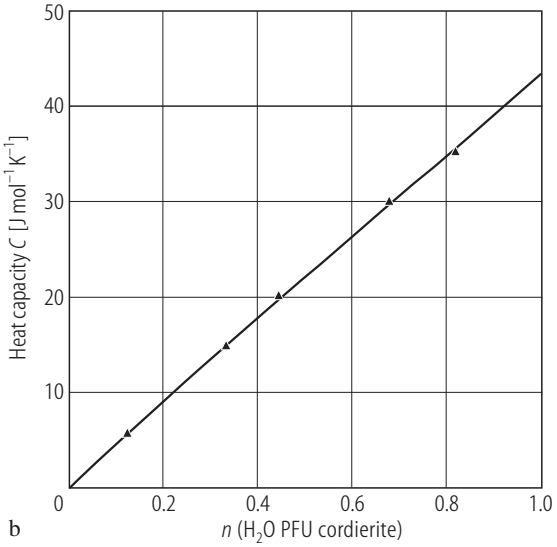

Fig. 19. Cordierites. **(a)** Heat capacity data for high and low structural state and glass from 295 to 425 K. **(b)** The difference in heat capacity between hydrous and anhydrous samples as function of H_2O content [93C1]. All data between 295 K and 425 K are included in the plot.

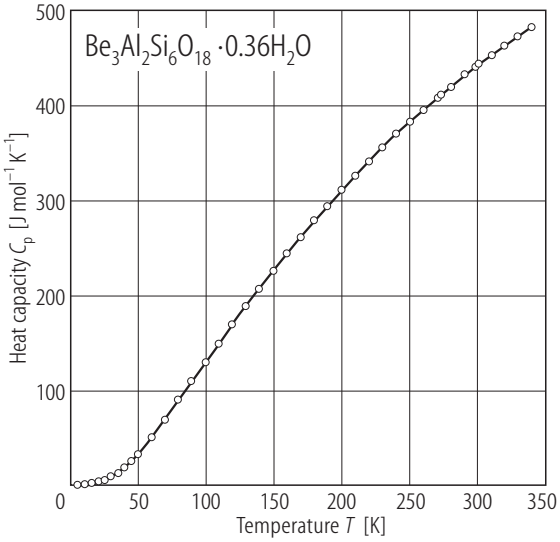

Fig. 20. Beryl. Temperature dependence of heat capacity [86H2].

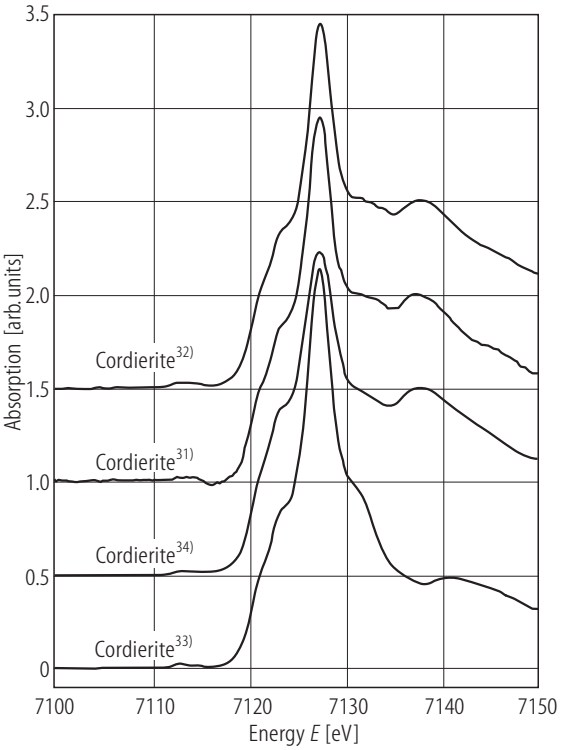

Fig. 21. Natural cordierites[31...34]. XAS spectra at room temperature [00G1] (for compositions [31...34]see Table 3).

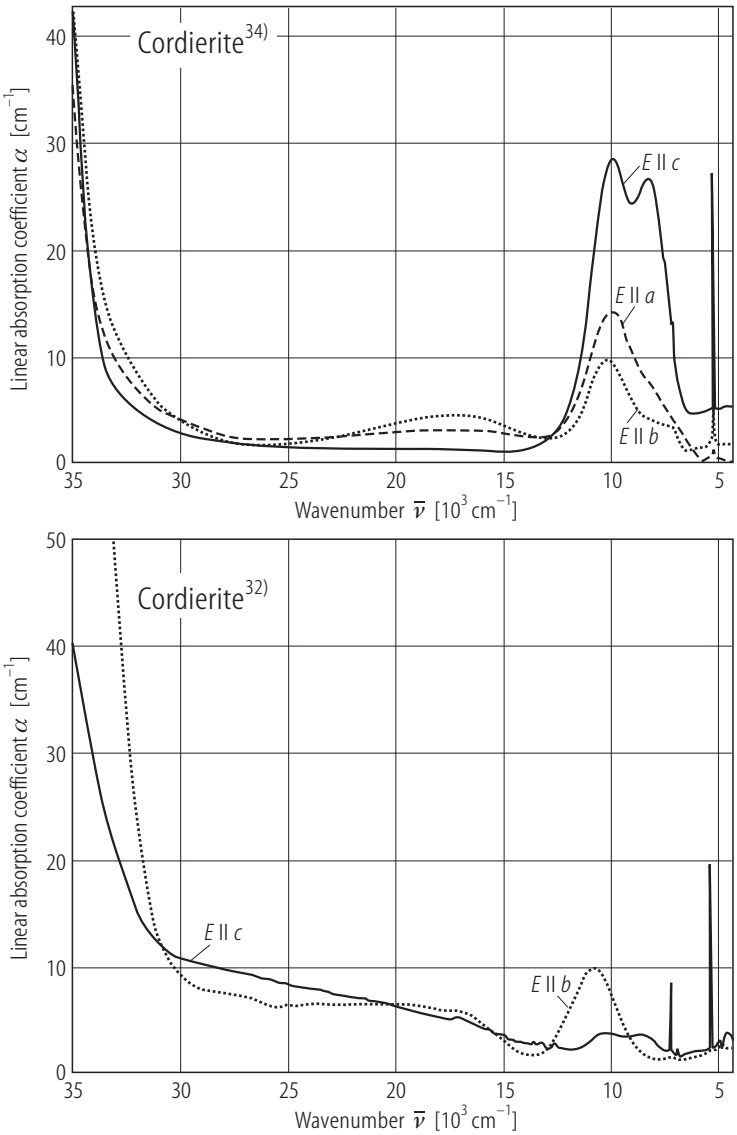

Fig. 22. Natural cordierites[32,34)]. Room-temperature polarized absorption spectra. The polarized directions are ***a***, ***b***, ***c*** [00G1] (for footnotes (compositions) [32,34)] see Table 3).

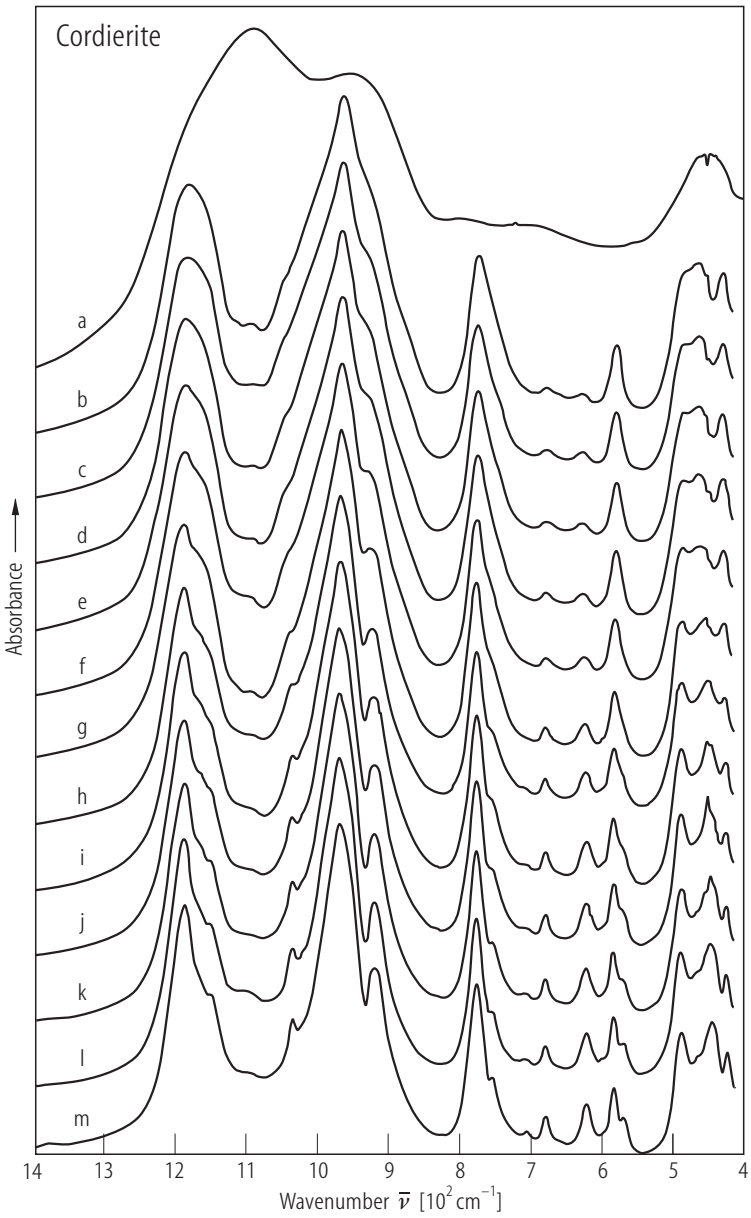

Fig. 23. Mg-cordierite glass and crystalline. IR spectra at RT of glass **(a)** and samples annealed at 1290ºC for different duration: **(b)** t = 2 min.; **(c)** t = 5 min.; **(d)** t = 10 min.; **(e)** t = 20 min.; **(f)** t = 40 min.; (**g**) t = 1 h; (**h**) t = 3 h; (**i**) t = 6 h; (**j**) t = 12 h; (**k**) t = 24 h; (**l**) t = 48 h; (**m**) t = 96 h. The symmetry of the cordierite samples is hexagonal for **b**, **c**, **d**, **e**, modulated for **f**, **g**, **h**, and orthorhombic for **i**, **j**, **k**, **l**, **m** [89G2].

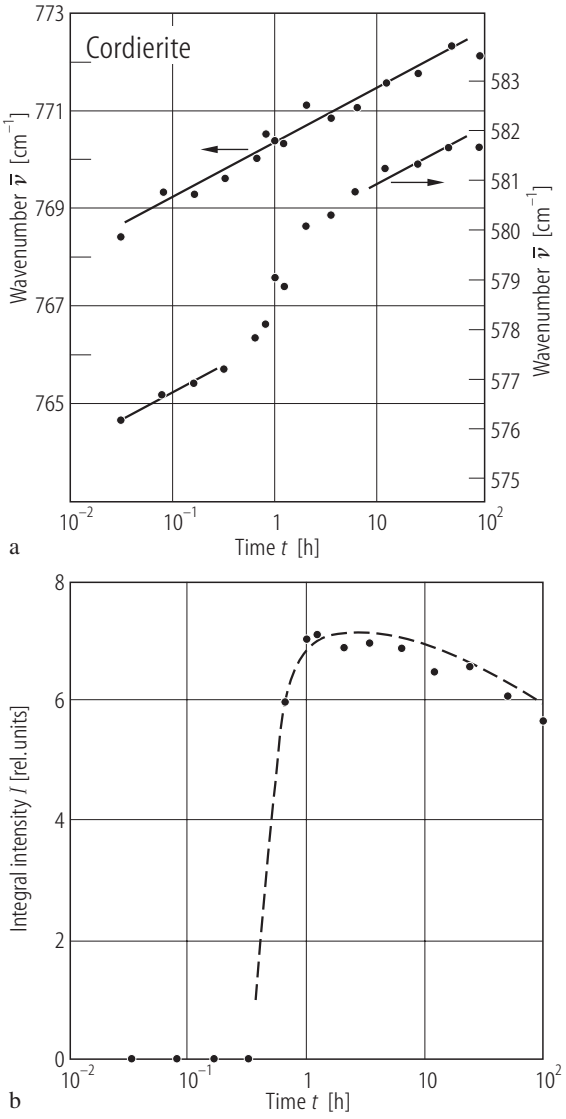

Fig. 24. Mg-cordierite. **(a)** Frequency shift versus logarithmic annealing time of the modes near 770 cm^{-1} and 580 cm^{-1} (from room-temperature measurements). **(b)** Integrated intensity vs logarithmic annealing time of the mode near 568 cm^{-1} as deduced by line profile analysis of the 80 K measurements [89G2].

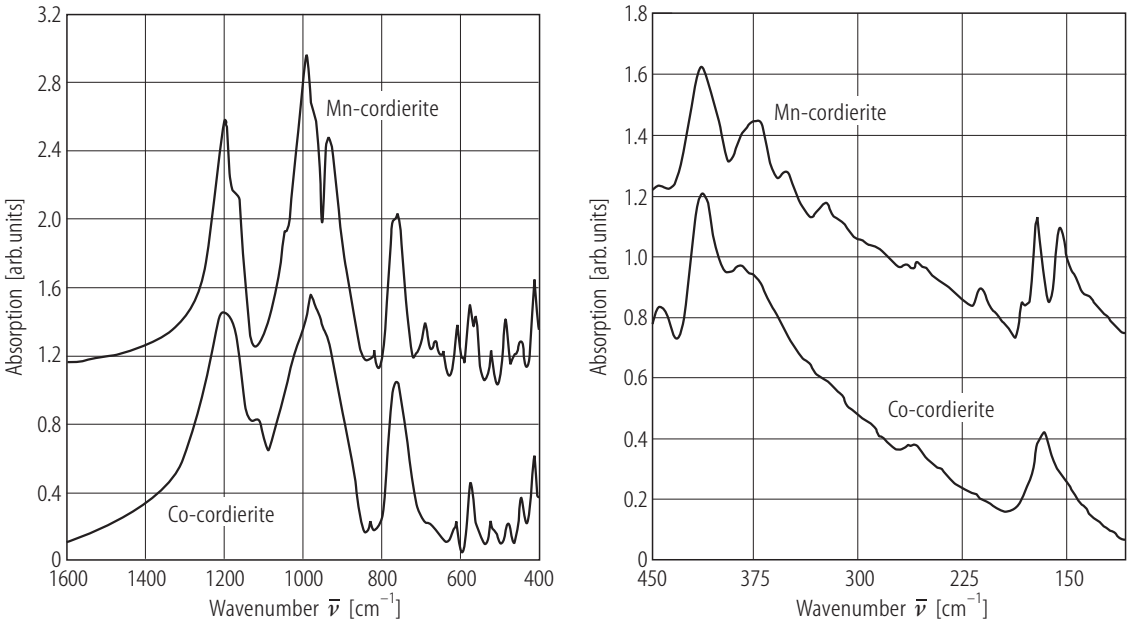

Fig. 25. Mn- and Co-cordierites. FTIR absorption spectra from 80…1600 cm^{-1}. The difference in the width of the absorption bands is due to the different ordering states [99K1].

For Fig. 26 see next page

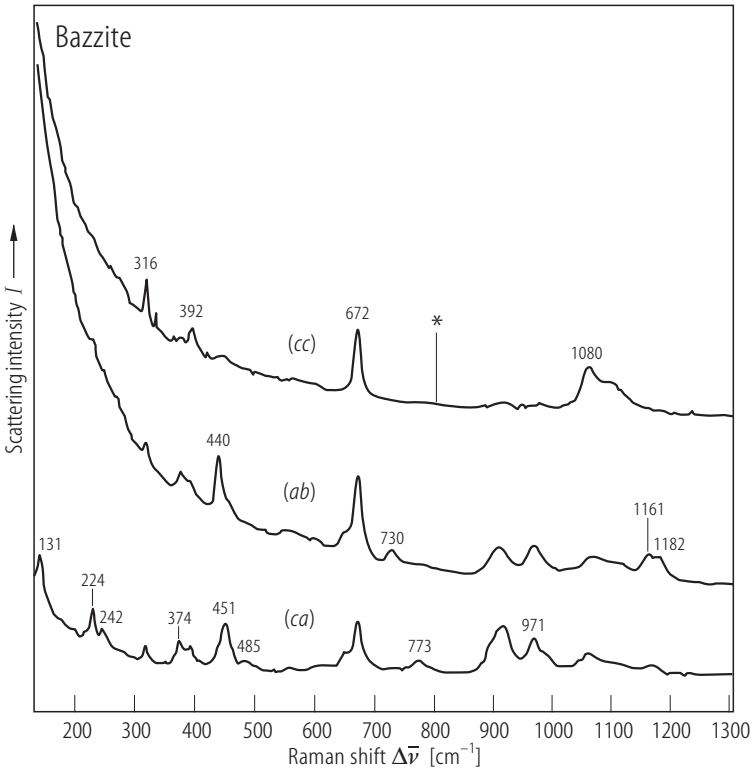

Fig. 27. Bazzite. Polarized Raman spectra at room temperature. The sharp peak marked * is an artefact and does not belong to the spectrum [90H1].

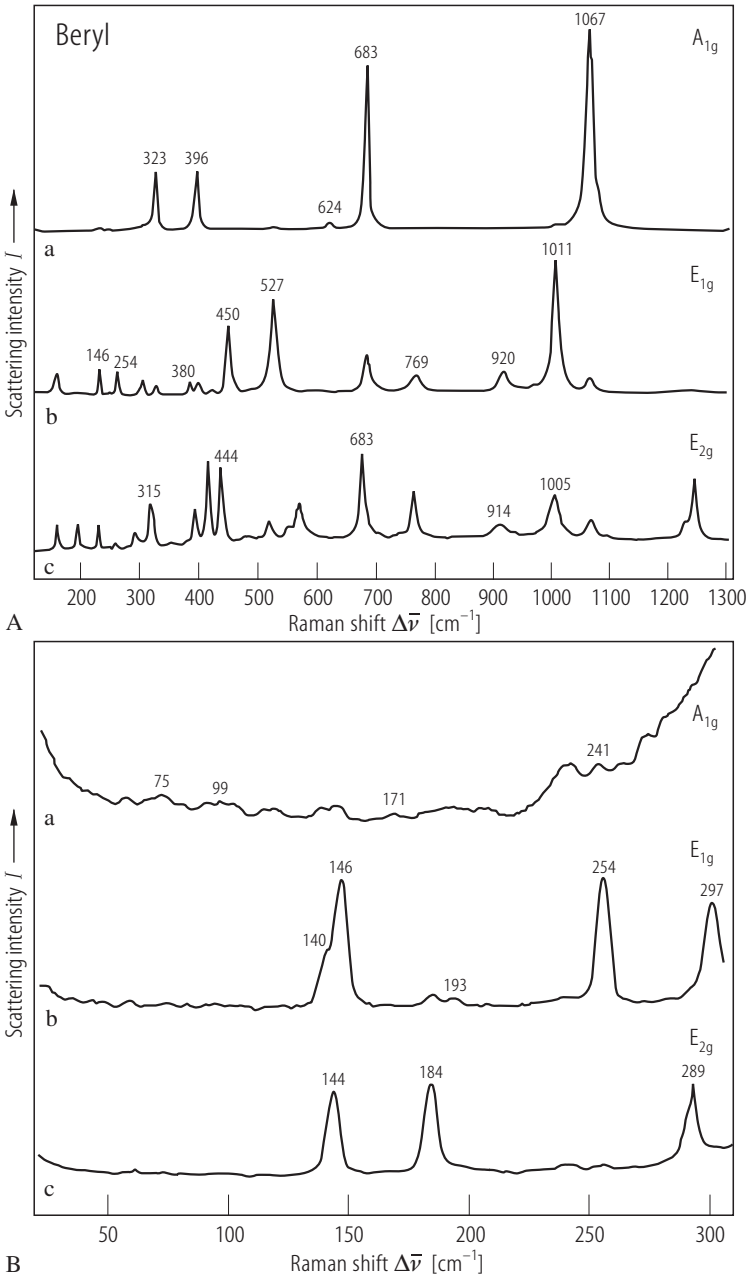

Fig. 26. Beryl. Polarized Raman spectra at room temperature in: **(a)** A_{1g} symmetry (polarization (*cc*)), **(b)** E_{1g} symmetry (polarization (*ca*)), **(c)** E_{2g} symmetry (polarization (*ba*)) [90H1]. (Sample: synthetic flux grown emerald (0.73 wt % Cr_2O_3)).

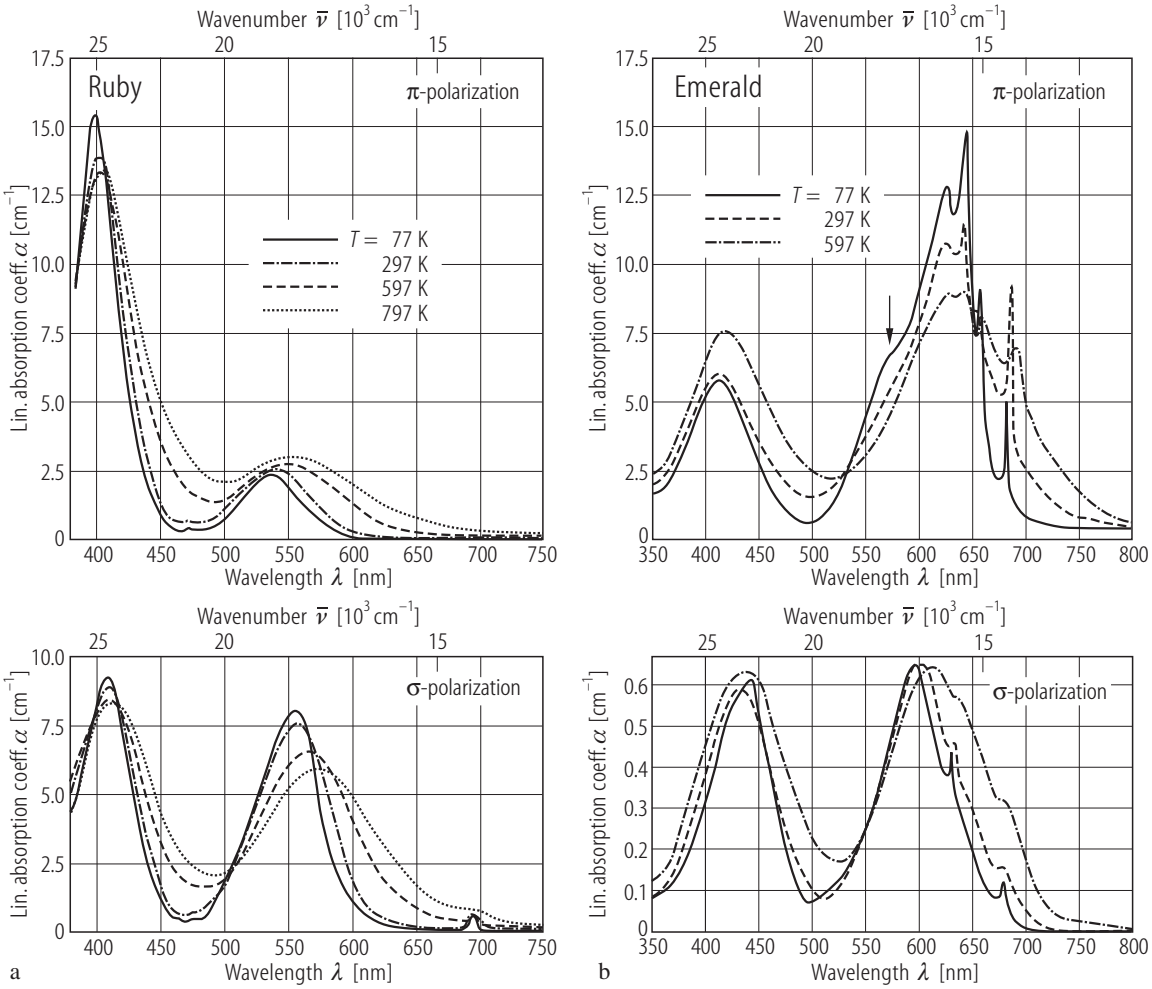

Fig. 28. Ruby **(a)** and emerald **(b)**. Polarized spectra $\boldsymbol{E} \parallel \boldsymbol{c}$ (π) and $\boldsymbol{E} \perp \boldsymbol{c}$ (σ) in the temperature range 77 to 597 K [94T1].

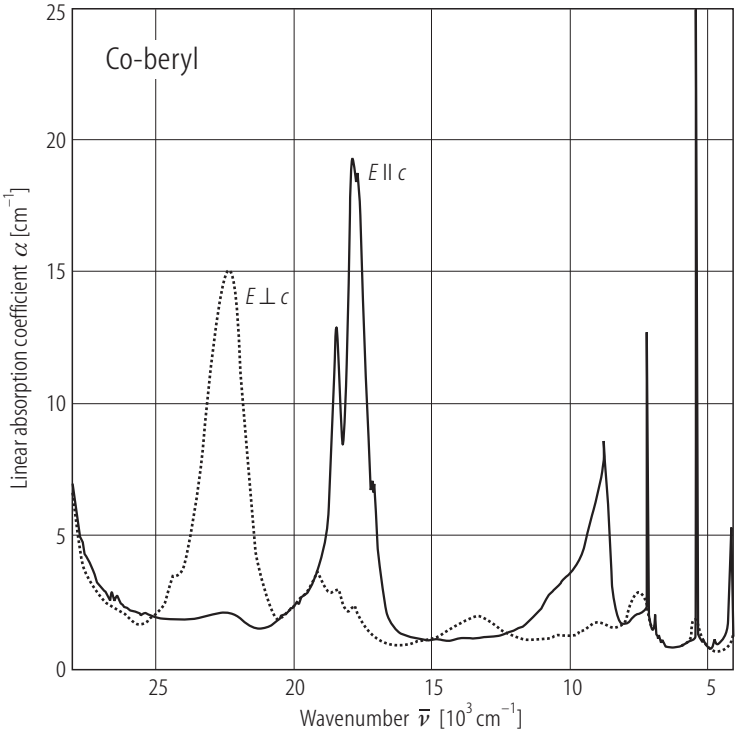

Fig. 29. Co-bearing beryl. Polarized optical absorption spectra [01T1].

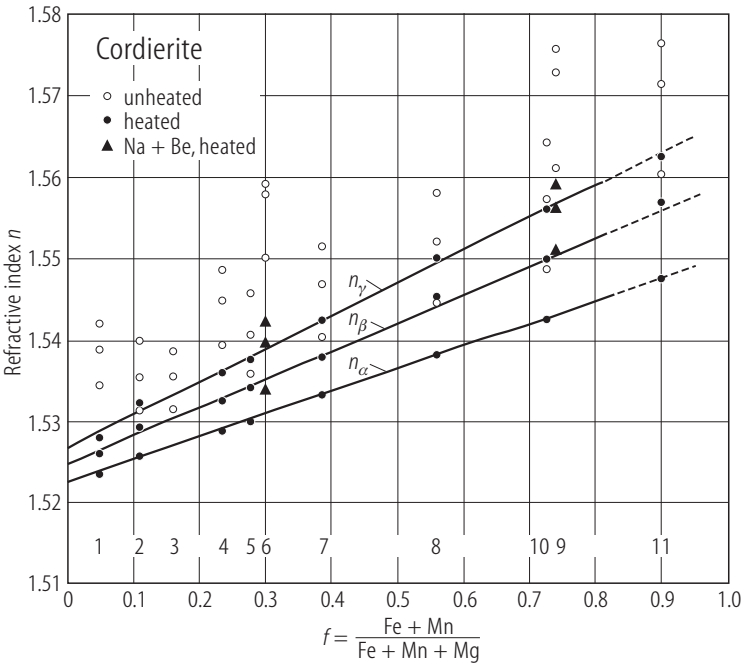

Fig. 30. Cordierites. Refractive indices n_α, n_β and n_γ versus atomic ratio f for unheated cordierite grains 1 to 11 (open circles) and for the same grains after heating at 800ºC for six hours (filled circles or triangles) [80S1].